Implications of the quaternary twist allosteric model for the physiology and pathology of nicotinic acetylcholine receptors

Antoine Taly*†, Pierre-Jean Corringer*, Thomas Grutter*, Lia Prado de Carvalho*, Martin Karplus‡§, and Jean-Pierre Changeux*¶

*Recepteurs et Cognition, Unité de Recherche Associée Centre National de la Recherche Scientifique 2182, Institut Pasteur, 25 Rue du Dr Roux, 75724 Paris Cedex 15, France; ‡Laboratoire de Chimie Biophysique, Institut de Science et d'Ingénierie Supramoléculaire, Université Louis Pasteur, 8, Allée Gaspard Monge, B.P. 70028, F-67083 Strasbourg Cedex, France; and §Department of Chemistry and Chemical Biology, Harvard University, 12 Oxford Street, Cambridge, MA 02138

Contributed by Jean-Pierre Changeux, September 12, 2006

Nicotinic acetylcholine receptors (nAChR) are pentameric ligand-gated ion channels composed of subunits that consist of an extracellular domain that carries the ligand-binding site and a distinct ion-pore domain. Signal transduction results from the allosteric coupling between the two domains: the distance from the binding site to the gate of the pore domain is 50 Å. Normal mode analysis with a C_α Gaussian network of a new structural model of the neuronal α7 nAChR showed that the lowest mode involves a global quaternary twist motion that opens the ion pore. A molecular probe analysis, in which the network is modified at each individual amino acid residue, demonstrated that the major effect is to change the frequency, but not the form, of the twist mode. The largest effects were observed for the ligand-binding site and the Cys-loop. Most (24/27) of spontaneous mutations known to cause congenital myasthenia and autosomal dominant nocturnal frontal lobe epilepsy are located either at the interface between subunits or, within a given subunit, at the interface between rigid blocks. These interfaces are modified significantly by the twist mode. The present analysis, thus, supports the quaternary twist model of the nAChR allosteric transition and provides a qualitative interpretation of the effect of the mutations responsible for several receptor pathologies.

allosteric transition | nicotinic receptor | pathological mutations | normal mode perturbation scanning

Nicotinic acetylcholine receptors (nAChRs) play a central role in intercellular communications in the brain and at the neuromuscular junction. They are involved in nicotine addiction as well as in cognitive processes such as attention, access to consciousness, learning, and memory, and their pathologies include autism, schizophrenia, Parkinson's disease, and Alzheimer's disease (references in ref. 1). Understanding the functional organization of the nAChR at the atomic level thus is of considerable interest in itself and is a source of insights for the development of new drug therapies.

nAChRs are members of the Cys-loop superfamily of ligand-gated ion channels. They are hetero- or homopentameric integral membrane proteins with a fivefold axis of pseudo-symmetry perpendicular to the membrane. Each subunit can be subdivided into two principal domains: extracellular and transmembrane. The extracellular domain (ECD) carries the acetylcholine (ACh) binding site at the boundary between subunits, and the transmembrane ion-pore domain (IPD) delineates an axial cation-specific channel (2, 3). These topologically distinct domains are coupled allosterically to each other. Therefore, nAChRs possess the structural elements necessary to convert a chemical signal, typically a local increase of extracellular ACh concentration, into an electrical signal generated by the opening of the ion channel.

Electrophysiological analysis of nAChRs has shown that rapid delivery of ACh promotes fast opening of the channel, and that a prolonged application of ACh leads to a slow decrease of the response amplitude or "desensitization." Several kinetic models have been proposed for the processes of activation and desensitization (4) as well as the structural transitions related to general mechanisms of allosteric transitions known to mediate signal transmission (see refs. 1, 5, and 6). The concerted Monod–Wyman–Changeux (MWC) model (7) has been extended to the nAChR. It is assumed that there is a reversible equilibrium between a basal state (B), an active open-channel state (A) stabilized by ACh and nicotinic agonists, and one or several high-affinity desensitized state(s) with a closed channel (D) (see refs. 1 and 5).

Using recent structural data from electron microscopy of the *Torpedo* muscle nAChR (8), we have constructed an improved model of the neuronal α7 nAChR [see Taly *et al*. (9) for the earlier model]. Normal mode analysis (NMA) performed by using a C_α Gaussian network confirms that the lowest frequency mode is a quaternary twist motion that opens the ion pore. In this article, we use a perturbation analysis of this mode to study *in silico* the structure/function relationships of the nAChR. A molecular probe was introduced by inserting additional atoms at each individual C_α. For certain residues, the modified network leads to a change of frequency of the twist mode without significant modification of its form. The largest effects of the perturbation were observed for the ligand-binding site, for the Cys-loop, and possibly for the Ca^{2+} allosteric site, which is in accord with their proposed role as dominant functional sites.

We then investigated certain spontaneous pathological mutations. We found that a significant number of them were located at the interface between subunits or at the interface between rigid blocks within a subunit identified earlier (9). The molecular probe data and the mutational analysis indicate that the quaternary twist model of gating proposed previously provides a meaningful description of the opening from B to A of the ion pore (9) and of the effect of pathological mutations.

Author contributions: A.T., M.K., and J.-P.C. designed research; A.T. performed research; P.-J.C., T.G., and L.P.d.C. analyzed data; and A.T., M.K., and J.-P.C. wrote the paper.

The authors declare no conflict of interest.

Freely available online through the PNAS open access option.

Abbreviations: ACh, acetylcholine; nAChR, nicotinic acetylcholine receptor; IPD, ion-pore domain; ECD, extracellular domain; NMA, normal mode analysis; ADNFLE, autosomal dominant nocturnal frontal lobe epilepsy.

†To whom correspondence may be sent at the present address: Laboratoire de Chimie Biophysique, Université Louis Pasteur, 8, Allée Gaspard Monge, B.P. 70028, F-67083 Strasbourg Cedex, France. E-mail: a.taly@isis.u-strasbg.fr.

¶To whom correspondence may be addressed. E-mail: changeux@pasteur.fr.

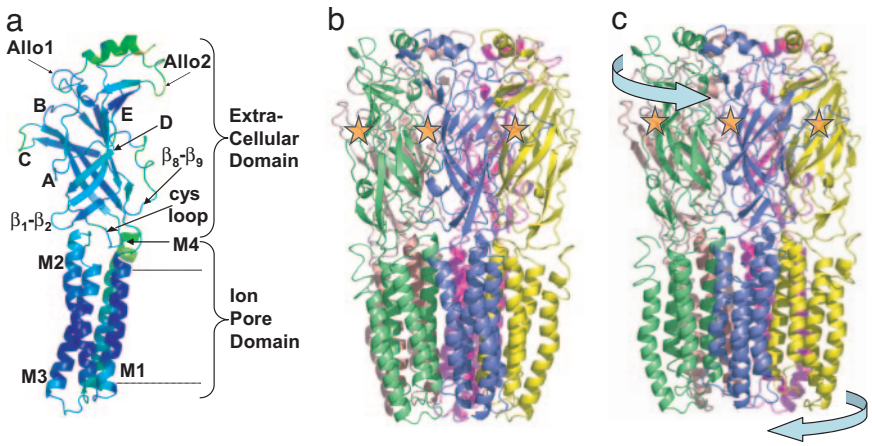

Fig. 1. Model structures and comparison. (*a*) Structure of one subunit of the present α7 nAChR model. The rmsd between the present and the previous model(s), computed for each atom, is displayed on the structure through a color coding from ≈2 Å (dark blue) to ≈10 Å (orange). (*b*) Present α7 nAChR model viewed from the membrane plane. A different color is used for each subunit. (*c*) Open-pore model obtained after exploration of the twist mode and energy minimization (see *Results and Discussion*). The comparison of *b* and *c* demonstrates the quaternary twist motion between the structures (following the arrows). Stars were added to help localize the binding sites.

Results and Discussion

NMA of the New α7 Model. ***Construction of a new α7 nAChR model.*** We have constructed a new model of the α7 nAChR by using the electron microscopy structure of *Torpedo* muscle receptor obtained at a 4-Å resolution (8). Whereas previously we used the structure of the ACh binding protein (AChBP) to model the ECD (9), the latest structure of the *Torpedo* receptor includes that domain. The electron microscopy data were proposed to represent a basal state of the nAChR protein (8), although this interpretation remains a matter of controversy (10). The reported structure of the muscle receptor, which has the composition $(\alpha 1)_2\beta 1\gamma\delta$, is asymmetric (8). Notably the C-loop of the α1 subunits is in an "open" conformation, whereas that of the other subunits is "closed." Opening of the C-loop previously was shown to be necessary for the binding of α-neurotoxins (11, 12), which generally is thought to take place in the basal state (13–15). Therefore, an α1 subunit of the *Torpedo* electron microscopy structure was chosen as the template to model nAChR α subunits in the basal state.

The structure of one α7 subunit was modeled by homology using the α1 subunit at the α_1/γ interface of the muscle receptor as a template (see *Supporting Text* for details and Fig. 4*a* for the alignment, both of which are published as supporting information on the PNAS web site). The resulting subunit was superimposed on the five subunits of our previous model (9) to form a pentamer. Energy minimization of the model was performed (9) (see *Supporting Text* for details). The final model of α7 nAChR is presented in Fig. 1*b*. It shows significant differences from the earlier model (9), although qualitatively it is quite similar (details are given in Fig. 1*a* and in the supporting information). In the present model, loop C is open (Fig. 4*b*), whereas it was closed over the binding site in the previous model (Fig. 4*c*). Given the above-described relation between the C-loop conformation and the receptor state, this observation is consistent with the notion that the present model describes the basal state of the receptor.

NMA of the present α7 model. NMA was performed as for the earlier model with a C_α Gaussian network (see the supporting information). The observed modes are different from those obtained with the previous model (see the supporting information for details) (9), except for the lowest mode, which has a large overlap. This mode corresponds to a global twist movement in both models.

Each mode was analyzed for its compatibility with a gating mechanism. First, we checked whether the modes were associated with a physical opening of the ion channel (see *Methods*). Only modes 1, 5, and 6 showed a significant opening of the pore. However, as modes 5 and 6 involve a strong bending deformation of the IPD, the allowed motion along these modes is expected to be much smaller than that for mode 1. The three structures associated with opening of the pore were tested for the change in accessibility of residue M1–213, which has been shown to become accessible during the gating (opening) process (16). Only mode 1 showed an increase of accessibility for that particular residue. Accordingly, we focus on the twist mode (mode 1) for an analysis of the physiological gating mechanism.

Some properties of the twist mode are given in *Supporting Results and Discussion* in *Supporting Text* (see also Fig. 5, which is published as supporting information on the PNAS web site). Because this mode opens the pore in both directions of displacement from the model structure, the direction that also increases the accessibility of residue M1–213 was used. The open-pore structure was taken as the one that opens the pore from ≈3 to ≈4 Å (Figs. 1*b* and 4*d*); it has an rmsd of ≈5 Å from the model structure.

We note that a twist mode is generally the lowest mode for such a cylindrical structure. What is important here is that this mode opens the pore and so can be associated with the gating mechanism. The normal modes obtained with another structure (9) and a different force field (17) have in common that the first mode is a twist mode; higher modes differ more. The fact that the twist mode is found with several setups supports the robustness of the results and the functional importance of the twist mode (18). It appears likely that the various receptors in the Cys-loop family share the same gating mechanism in accord with experimental data; e.g., it is possible to construct a functional receptor by coupling the ECD and the IPD from evolutionary distant proteins (19, 20).

Normal Mode Perturbation Scanning. To identify sites of the protein that can alter the gating mechanism corresponding to the twist mode, we studied the effect of a local perturbation on each of its residues (21, 22). Given the simple model we were using, we added atoms to each C_α so as to locally modify the elastic network (see *Methods*) (a test case for the perturbation model is presented in the *Supporting Text* and Figs. 6 and 7, which are published as supporting information on the PNAS web site). The

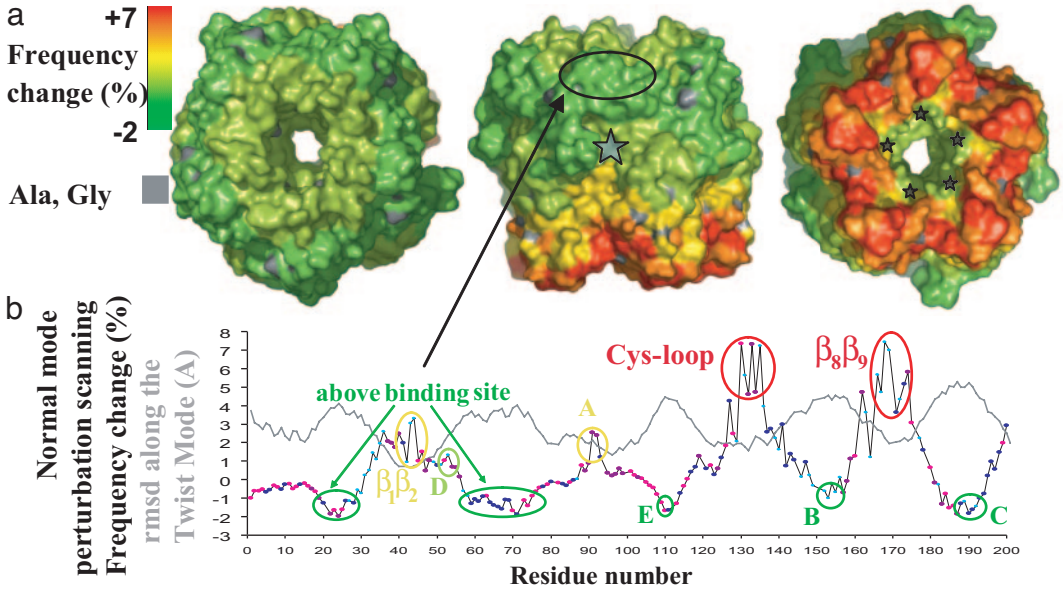

Fig. 2. Application of normal mode perturbation scanning on the twist mode in nAChR. (*a*) The ECD is viewed from the top (*Left*), membrane (*Center*), and bottom (*Right*). The results are represented on the structure through a color coding: the change in frequency range from −2% (green) to +7% (red). Ala and Gly, for which the probe was not constructed, appear in light gray. The star indicates the binding site. (*b*) Plot, as a function of residue numbers, of (*i*) the rmsd between the initial and pore-open structures and (*ii*) the change in frequency caused by the probe. The residues are colored depending on their position relative to the interfaces: interface between subunits, pink; interface between rigid blocks, cyan; both interfaces, violet; and none of the interfaces, dark blue (see definition in *Methods*).

resulting modification of the network mimics the effect of binding a ligand or introducing a mutation.

In the elastic model, the probe could produce two types of effects on the twist mode: modifications of (*i*) the frequency of the mode and/or (*ii*) the nature of the mode. We find that the normalized correlation coefficient between the perturbed modes and the unperturbed mode is 0.977 to 1.00 (see *Methods*). Thus, the change in frequency of the mode caused by the additional atoms is the essential effect, which we consider in what follows. We note that the correlation coefficient is related inversely to the positional rmsd along the twist mode. Accordingly, the cytoplasmic half of M1, which shows the largest rmsd, also has the lowest correlation coefficient (0.977–0.998). In the ECD, loop C (see Fig. 1*a*) is the zone with the lowest correlation coefficient (0.988–0.995), in accord with the fact that it has an open conformation and is therefore a highly flexible region of the ECD.

Sizeable effects of the probe were found in both the ECD and the IPD. For the IPD, large positive values were obtained at the top of M1 (+18%) and in the M2–M3 loop (+10%), which participate in the coupling between the ECD and the IPD, and a large negative value (−4%) was observed at the bottom of the IPD, in particular at the M1–M2 loop, which is believed to constitute the gate. However, we note that the magnitude of the probe effect might be unreliable because it has been shown that, in the presence of a membrane, the first mode is similar but the movements of the major part of the IPD (helices M1, M3, and M4) are of smaller amplitude (17). Therefore, the results could be quantitatively biased while remaining qualitatively correct.

In the ECD, the change in frequency caused by the probe ranged from −2% to +7%. The results are represented on the surface of the ECD by color coding (Fig. 2*a*). Two zones of the ECD show large positive values: the Cys-loop and β_8–β_9 loop, which are both at the interface between the ECD and the IPD. The interface between ECD and IPD is the boundary between (+) and (−) twisting and was found previously to correlate with the bending hinge of the twist mode (9). Interestingly, these large positive frequency changes, as well as those in the IPD, correspond to regions of low rms displacements in the twist mode (see Fig. 2). This finding suggests that the packing effects tend to make the frequency sensitive to the perturbation.

The five zones that have negative values are grouped in one area that includes loops that form the binding site (B, C, and E; see Fig. 1*a* for the position of loops) and two loops above the binding site. These "loops" are generally the connections between two β-strands. The previously unidentified loops, which we refer to as Allo1 (residues 20–28) and Allo2 (residues 58–77) (see Fig. 1*a*), contribute, with the B, C, and E loops, to the interface between subunits (Figs. 1*a* and 2*b*). It is interesting that additional connectivity in these regions softens the twist mode, so as to lower the energy of motion along it. If an analogous effect occurred in actually binding a ligand, it would be in accord with the increase in entropy calculated for other systems (23).

In addition to the above, visual inspection of the color-coded surface (Fig. 2*a Right*) shows that there is a small patch of residues that has perturbation values close to zero, next to the Cys-loop and the β_8–β_9 loop, both of which show largely positive values. The residues (residues 40–45) are yellow/light green, except residue 44, which is orange. Interestingly, these residues have been proposed to mediate the effect of calcium on nAChR gating (residues 40, 42, 43, and 171) (12).

The analysis of the effect of the probe on the frequency of the twist mode thus has revealed three key functional sites: (*i*) the Cys-loop and the β_8–β_9 loop; (*ii*) the ligand-binding site; and (*iii*) the Ca^{2+} allosteric site. The Cys-loop has been shown recently to regulate the gating of the receptor (19, 20, 24), and the β_8–β_9 loop has been shown also to participate in the gating between the ECD and IPD (19). The ligand and Ca^{2+} binding

NEUROSCIENCE

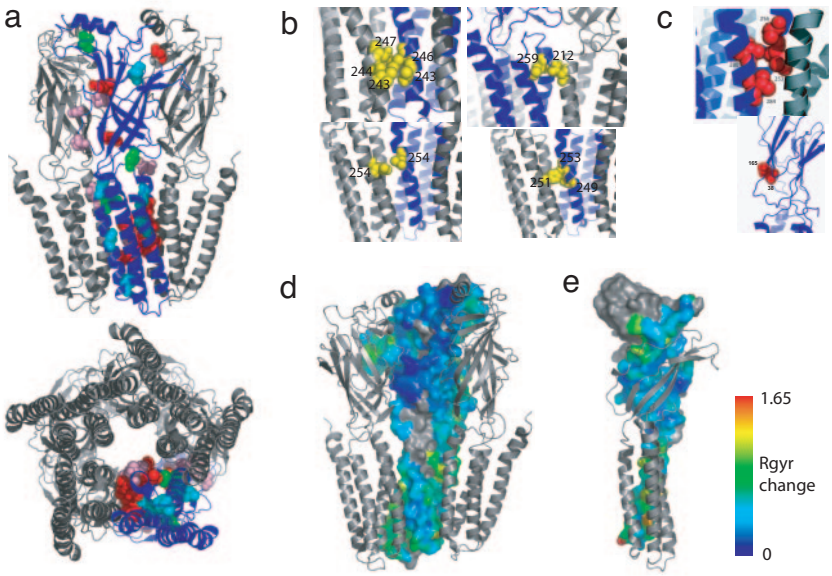

Fig. 3. Analysis of mutations associated with congenital myasthenia and ADNFLE. (*a–c*) Mutated residues at subunit interfaces are shown in pink, those at domain interfaces are shown in cyan, those at both interfaces are shown in red, and the others are shown in green. (*a*) All mutated residues. (*b*) Close view of the pairs identified as involving mutated positions at the interfaces between subunits (see text). (*c*) Close view of the pairs of mutation positions at the interface between dynamic domains (see text). (*d*) Illustration of the part of the interface between subunits that changes along the twist mode. The subunit at the center is displayed with a surface representation. The local movement in the twist mode (see *Methods*) is represented by a color coding for the portion of the surface that is <5 Å from the other subunits (shown in cartoon representation and colored in gray). (*e*) Illustration of the interface between rigid blocks; ''internal block'' is displayed with a surface representation. The local movement in the twist mode (see *Methods*) is represented by a color coding for the portion of the surface that is <5 Å from the ''external block'' (shown in cartoon representation and colored in gray).

sites are known to regulate the gating of the receptor through ligand/ion binding (12). The possibility of finding known allosteric sites by a perturbation analysis, reinforces the idea that the twist mode describes the gating mechanism of the nAChR.

Relation Between the Twist Mode and *in Vivo* Pathological Mutations. Several naturally occurring mutations of the nAChR promote a change in the gating properties of the receptor. A set of well studied mutations of neuronal and muscular nAChRs are associated with autosomal dominant nocturnal frontal lobe epilepsy (ADNFLE) (25) and congenital myasthenia (26), respectively (see Table 1, which is published as supporting information on the PNAS web site). We mapped all mutations onto a single α7 subunit model and found that they are distributed on both the extracellular and transmembrane domains, with many on M2 (Fig. 3*a*). As already discussed (1), this wide distribution suggests an allosteric effect of the mutations; i.e., the mutations are likely to alter the equilibrium between discrete states (open and closed) rather than have a specific local effect.

Pathological phenotypes cannot be predicted directly by the molecular probe analysis, which is meaningful only for regions of the protein rather than for individual residues. However, we did find that the mean effect of the probe on the twist mode was larger for the tested mutation positions (+3.56%) than for the whole protein (+1.33%; $\alpha < 0.01$; the statistical analyses are detailed in *Supporting Text* and the number of residues in each category is shown in Table 2, which is published as supporting information on the PNAS web site). We therefore investigated the possibility that the twist mode can be used to understand the origin of the pathological mutations. The present analysis does not distinguish between a gain or loss of function, which would require a more detailed model.

The localization of mutations on the structure is represented in Fig. 3*a*. A significant number of mutations were found localized at the interfaces between subunits and between rigid blocks (dynamic domains within subunits) (Fig. 8, which is published as supporting information on the PNAS web site). In the present α7 model, 24 of 27 mutations (89%) are at interfaces (see *Methods* for the definition of interface residues). This proportion should be compared with the value of 202 of 313 (65%) for the other residues ($\alpha < 0.02$). Thus, there is a bias for the pathogenic mutations to be located at the interfaces between the subunits and rigid blocks. The interfaces between subunits and between dynamic domains within subunits are regions where significant changes are introduced by motion along the twist mode (Fig. 3 *d* and *e* and Fig. 9, which is published as supporting information on the PNAS web site). The presence of mutations at these interfaces supports the conclusion that the quaternary and tertiary changes due to the twist mode play a role in the gating mechanism.

To look more specifically for interactions that could be modified by the twist mode, we examined whether some of the natural mutations are located <5 Å apart. This relatively large value was chosen to take into account interactions such as salt bridges or hydrogen bonds and to allow for uncertainties in the positions of the atoms from errors in the model. Pairs of residues thus identified are presented in Fig. 3 *b* and *c* and are listed in Table 1. First, there are pairs of residues in different subunits in positions corresponding to those in myasthenic mutations (M2–244/M2–246, M2–249/M2–251; the residue numbers are given according to the α7 numbering). Two pairs consist of residues that are in the same position in two adjacent subunits: one is from myasthenia (M2–254) and the other one is from ADNFLE (M2–243). Second, we observed pairs (M1–212/M2–259, M2–246/M2–247, and M2–251/M2–253), one of which correspond to myasthenia and the other to ADNFLE. We also found intrasubunit interactions (Fig. 3*c*): a pair inside

the ECD (38/165) and a cluster of hydrophobic residues inside the IPD (M3–280/M2–253, M3–284/M2–253, and M3–280/M2–256).

For each pair in a subunit interface, we computed the change in distance between the α-carbons of the residues from two subunits going in from the initial structure (Fig. 1*b*) to the open-pore structure (Fig. 1*c*) of the gating mode (see *Methods*). The changes in distance are sizable (from 1.71 to 6.36 Å; Table 1). This finding suggests that the specific interactions between subunits are altered during gating. However, the exact values should be taken with care because of the crudeness of the model and the possibility that the movement of helices M1, M3, and M4 may be overestimated, as discussed above.

It has been proposed that natural mutations alter the equilibrium between the functional states of the protein and result in altered kinetics (27, 28). The present analysis, which shows that interaction between residues at the interface and the distance between them vary during gating, supports such a model. Accordingly, the mutations would affect one conformation more than the other and consequently would modify the equilibrium and/or kinetics of interconversion between them.

Pathological mutations are being discovered continuously. A possible use of the model would be to propose potential myasthenic or ADNFLE mutations or mutations for testing *in vitro*. One such approach points to pairs of mutation for which similar effects would be obtained when each member of a pair is mutated. Extrapolating the results obtained with the homomeric α_7 to the situation of both the heteromeric $\alpha4\beta2$ and the muscle receptors, where two members of the pair are not adjacent, suggests additional mutations. Also, for mutations at the interface, but not forming a pair, additional potential mutation sites that interact with existing ones could be of interest (see the supporting information). Experimental exploration of such mutations is left for the future.

In other receptors from the Cys-loop family, positions corresponding to any of the pathological mutation already discussed might be pathogenic as well. We tested this hypothesis by analyzing six mutations of the glycine receptor that are associated with the hyperekplexia pathology (see the supporting information). It was found that Q266H, R271Q/L, and Y279C/S in the glycine receptor correspond to F251, A256, and D264 respectively, in the α_7 nicotinic receptor, which are homologous to pathological positions (see Table 1).

Conclusion

We have performed a NMA with an improved model of the neuronal α7 nAChR based on the recent structure of the *Torpedo* nAChR. It showed, in agreement with earlier work, that the lowest mode is a quaternary twist motion that opens the ion pore. An *in silico* perturbation that mimics ligand binding or amino acid mutation was used to probe the twist mode and resulted in the identification of the ligand-binding site, the Cys-loop, and the Ca^{2+} allosteric site as dominant functional sites. We have also studied the effect of known pathological and gain and loss of function mutations, and we found that most of them are located at the interface between subunits or between rigid blocks within subunits and that many of them form pairs on different sides of the interface. These are regions that are altered significantly by displacements along the twist mode. Together, the molecular probe data and the mutation analysis bring functional information supporting the quaternary twist mode for gating for α7 nAChR. The interfaces between the subunits are altered by the quaternary changes, and the interfaces between dynamic domains within a subunit are altered by the tertiary changes associated with the twist mode.

A corresponding analysis based on structural data, homology modeling, normal mode calculations, and perturbation probes could be applied to other receptors of the Cys-loop class. Also, the method could be used more generally. For example, the signal transduction mechanism of opioid receptor (G protein-coupled receptor) has been studied with 30 independent constitutive mutations identified from random mutagenesis experiment (29). If these mutations are widely distributed in the structure, in agreement with our views, many of them do form clusters.

Methods

Initial Model. The all-heavy-atom structure of the α_1 subunit from the muscular nAChR (Protein Data Bank ID code 2BG9) was taken as the template to construct the initial model with the program MODELLER (30) by using the alignment provided in Fig. 4*a*. The modeled α7 subunit was then projected fivefold. The resulting model was energy-minimized by using the program CHARMM (31, 32) with the all-atom param22 parameter set; the solvent was represented implicitly with a distance-dependant dielectric constant. The minimization protocol included a fivefold averaging (for details see the supporting information).

NMA. The gating mechanism was studied by NMA, as previously described (9), with a C_α elastic-network model (33), which represents the protein as a network of residues linked by springs. The computation was further sped up by a block normal mode calculation (34, 35) with blocks of size 5. The 100 lowest frequency modes were calculated.

To examine the normal modes, the positions of the C_α were modified along the normal mode vectors. The new positions of the C_α were introduced, while retaining the positions of the other atoms. The position of those atoms then were adjusted by energy minimization using decreasing harmonic constraints (see the supporting information for details) with the program CHARMM (31, 32).

Correlation Coefficient. We compared modes by computing a normalized correlation coefficient between the eigenvectors for each C_α, i.e., the cosine of the angle between the two sets of vectors. The value of this cosine is close to 1 (or -1) when two modes are highly correlated and close to 0 when the modes are unrelated.

Analysis of the Structures. Each mode was explored in both directions until an rmsd of $\approx$5 Å from the initial structure was obtained to determine the nature of the structural change involved.

The size of the pore was measured by using the program HOLE (36) with the classical bondi.rad radius definitions (37) and the Connoly algorithm (38). This combination gives a radius of 3 Å for the initial structure, which corresponds to the experimental radius for the closed channel. The accessibility of residue M1–213 was determined by using the program DSSP (39).

Analysis of the Zones That Display the Highest Mobility. By using CHARMM for each atom in the initial structure, all atoms within 5 Å were selected, and the radius of gyration of that selection was computed. Then, in the pore-open structure, the increase of the radius of gyration was computed. The result was fivefold averaged and stored for later display with pymol (40).

Sensitivity Probe. At the level of each residue, the probe was modeled by introducing five atoms in addition to the C_α. This number was chosen to match the size of one block. The atoms were C, N, and O from the backbone, the Cβ, and the following

heavy atom ("CG," except "CG1," for Ile and Val; "SG" for Cys; "OG" for Ser; and "OG1" for Thr). Gly and Ala, which lack additional heavy atoms, apart from the backbone, were excluded from the calculation. The probe was applied simultaneously to the five subunits. The change in frequency of the mode caused by the presence of the probe was computed and stored in the temperature factor for later display with pymol (40).

Interface Between Subunits. Interface residues were obtained from the Protein–Protein Interaction Server (www.biochem.ucl.ac.uk/bsm/PP/server). The accessible surface area is calculated as the surface mapped out by the center of a probe of radius 1.4 Å. The calculation is performed successively for the pentamer and a monomer. Interface residues are defined as the residues for which the accessible surface area decreases by >1 Å upon complexation.

We thank Oliver Smart for providing the program HOLE and M. Delarue, M. Spichty, and R. Stote for helpful discussion. This work was supported by the Balzan Foundation, the Association Française contre les Myopathies, and a postdoctoral fellowship from the Philip Morris External Research Program (to A.T.).

1. Changeux JP, Edelstein SJ (2005) *Nicotinic Acetylcholine Receptors* (Odile Jacob, New York).
2. Corringer PJ, Le Novere N, Changeux JP (2000) *Annu Rev Pharmacol Toxicol* 40:431–458.
3. Wilson G, Karlin A (2001) *Proc Natl Acad Sci USA* 98:1241–1248.
4. Katz B, Thesleff S (1957) *J Physiol* 138:63–80.
5. Edelstein SJ, Changeux JP (1996) *Experientia* 52:1083–1090.
6. Perutz MF (1989) *Q Rev Biophys* 22:139–237.
7. Monod J, Wyman J, Changeux JP (1965) *J Mol Biol* 12:88–118.
8. Unwin N (2005) *J Mol Biol* 346:967–989.
9. Taly A, Delarue M, Grutter T, Nilges M, Le Novere N, Corringer PJ, Changeux JP (2005) *Biophys J* 88:3954–3965.
10. Paas Y, Cartaud J, Recouvreur M, Grailhe R, Dufresne V, Pebay-Peyroula E, Landau EM, Changeux JP (2003) *Proc Natl Acad Sci USA* 100:11309–11314.
11. Fruchart-Gaillard C, Gilquin B, Antil-Delbeke S, Le Novere N, Tamiya T, Corringer PJ, Changeux JP, Menez A, Servent D (2002) *Proc Natl Acad Sci USA* 99:3216–3221.
12. Le Novere N, Grutter T, Changeux JP (2002) *Proc Natl Acad Sci USA* 99:3210–3215.
13. Bertrand D, Devillers-Thiery A, Revah F, Galzi JL, Hussy N, Mulle C, Bertrand S, Ballivet M, Changeux JP (1992) *Proc Natl Acad Sci USA* 89:1261–1265.
14. Moore MA, McCarthy MP (1995) *Biochim Biophys Acta* 1235:336–342.
15. Middleton RE, Strnad NP, Cohen JB (1999) *Mol Pharmacol* 56:290–299.
16. Zhang H, Karlin A (1997) *Biochemistry* 36:15856–15864.
17. Cheng X, Lu B, Grant B, Law RJ, McCammon JA (2006) *J Mol Biol* 355:310–324.
18. Nicolay S, Sanejouand YH (2006) *Phys Rev Lett* 96:078104.
19. Bouzat C, Gumilar F, Spitzmaul G, Wang HL, Rayes D, Hansen SB, Taylor P, Sine SM (2004) *Nature* 430:896–900.
20. Grutter T, Prado de Carvalho L, Dufresne V, Taly A, Edelstein SJ, Changeux JP (2005) *Proc Natl Acad Sci USA* 102:18207–18212.
21. Zheng W, Brooks BR, Doniach S, Thirumalai D (2005) *Structure (London)* 13:565–577.
22. Ming D, Wall ME (2005) *Phys Rev Lett* 95:198103.
23. Grunberg R, Nilges M, Leckner J (2006) *Structure (London)* 14:683–693.
24. Lummis SC, Beene DL, Lee LW, Lester HA, Broadhurst RW, Dougherty DA (2005) *Nature* 438:248–252.
25. Steinlein OK (2004) *Nat Rev Neurosci* 5:400–408.
26. Engel AG, Sine SM (2005) *Curr Opin Pharmacol* 5:308–321.
27. Edelstein SJ, Schaad O, Changeux JP (1997) *C R Acad Sci Ser III* 320:953–961.
28. Changeux J, Edelstein SJ (2001) *Curr Opin Neurobiol* 11:369–377.
29. Decaillot FM, Befort K, Filliol D, Yue S, Walker P, Kieffer BL (2003) *Nat Struct Biol* 10:629–636.
30. Sali A, Blundell TL (1993) *J Mol Biol* 234:779–815.
31. Brooks B, Karplus M (1983) *Proc Natl Acad Sci USA* 80:6571–6575.
32. MacKerell ADJ, Brooks B, Brooks CLI, Nilsson L, Roux B, Won Y, Karplus M (1998) in *The Encyclopedia of Computational Chemistry*, ed von Ragué Schleyer P (Wiley, Chichester, UK), pp 271–277.
33. Tirion MM (1996) *Phys Rev Lett* 77:1905–1908.
34. Tama F, Gadea FX, Marques O, Sanejouand YH (2000) *Proteins* 41:1–7.
35. Tama F, Sanejouand YH (2001) *Protein Eng* 14:1–6.
36. Smart OS, Neduvelil JG, Wang X, Wallace BA, Sansom MS (1996) *J Mol Graph* 14:354–360, 376.
37. Bondi A (1964) *J Phys Chem* 68:441–451.
38. Connolly ML (1983) *Science* 221:709–713.
39. Kabsch W, Sander C (1983) *Biopolymers* 22:2577–2637.
40. DeLano WL (2002) *pymol* (DeLano Scientific, San Carlos, CA).